

# Null-stream veto for two co-located detectors: Implementation issues

P Ajith<sup>†</sup>, M Hewitson<sup>†</sup> and I S Heng<sup>‡</sup>

<sup>†</sup> Max-Planck-Institut für Gravitationsphysik (Albert-Einstein-Institut) und Universität Hannover, Callinstr. 38, 30167 Hannover, Germany

<sup>‡</sup> Department of Physics and Astronomy, University of Glasgow, Glasgow, G12 8QQ, United Kingdom

E-mail: Ajith.Parameswaran@aei.mpg.de

## Abstract.

Time-series data from multiple gravitational wave (GW) detectors can be linearly combined to form a *null-stream*, in which all GW information will be cancelled out. This null-stream can be used to distinguish between actual GW triggers and spurious noise transients in a search for GW bursts using a network of detectors. The biggest source of error in the null-stream analysis comes from the fact that the detector data are *not* perfectly calibrated. In this paper, we present an implementation of the null-stream veto in the simplest network of two co-located detectors. The detectors are assumed to have calibration uncertainties and correlated noise components. We estimate the effect of calibration uncertainties in the null-stream veto analysis and propose a new formulation to overcome this. This new formulation is demonstrated by doing software injections in Gaussian noise.

## 1. Introduction

Given the time series data from a network of gravitational-wave (GW) detectors, one can find a particular linear combination of the data streams such that it does not contain any trace of GWs. The idea of this *null-stream* was proposed by Gürsel and Tinto in their classic work [1]. Gürsel and Tinto proposed that the null-stream can be used to solve the ‘inverse problem’ of GW bursts, i.e., to compute the unknown quantities (two sky-positions and two polarizations) associated with the gravitational-waveform from the responses of three broad-band detectors.

Recently, there has been a lot of interest in the null-stream among the GW community. The main reason for this rejuvenated interest is that the first generation of ground-based interferometric GW detectors [2, 3, 4, 5] have started acquiring scientifically interesting data. Among the most promising astrophysical sources of GWs for these ground-based detectors are the transient, unmodelled astrophysical phenomena like supernovae explosions, Gamma-ray bursts and black hole/neutron star mergers - popularly known as ‘unmodelled bursts’. Most of the algorithms currently used in burst-searches are time-frequency detection algorithms that look for short-lived excitations of power in the ‘time-frequency map’ constructed from the data [6, 7, 8]. Since present-day interferometric GW detectors are highly complex instruments, the data often contains lots of noise transients which trigger the burst

detection algorithms. It is almost impossible to distinguish these spurious instrumental bursts from actual GW bursts using any physical model of the GW bursts. Thus, burst-data-analysis is usually performed as a coincidence analysis between multiple detectors. Although this ‘coincidence requirement’ considerably reduces the list of candidate burst triggers, one month of data can potentially produce hundreds of multi-detector random coincidences. So, it becomes absolutely necessary to have additional ‘waveform consistency tests’ that distinguish actual GW bursts from spurious noise transients. A cross-correlation statistic that is formulated in [9] is already being used as a coherent waveform consistency test in the search for GW bursts in the data of LIGO detectors. This is making use of the fact that all the LIGO detectors are aligned (approximately) parallel to each other.

Recently, it was proposed by [10] that the null-stream can be used to distinguish between actual GW triggers and spurious noise transients in a search for GW bursts using any general network of detectors. The main idea is that, if the coincident triggers correspond to an actual GW burst, the null-stream constructed at the time of the triggers will contain no trace of the burst, and, will fall in to an expected noise-distribution. On the other hand, if the coincident triggers correspond to spurious instrumental bursts, the bursts will not necessarily cancel out in the null-stream, and the null-stream will contain some excess power. Many authors have proposed similar, but non-equivalent ways of implementing this. Our method is based on the *excess power* statistic [6], which was first used by [10] in this context. This method is formally developed and is studied in detail in [11]. For an alternative implementation, see [12]. A similar veto strategy using the null-stream constructed from the two calibrated output quadratures of GEO 600 [4] detector is already being used to veto the burst triggers from GEO 600. This is discussed in [13].

It was soon realised that the biggest source of error in the null-stream analysis comes from the fact that the detector data are *not* perfectly calibrated, due to various reasons. In such cases, the null-stream constructed from the data containing actual GW bursts will contain some residual signal and will deviate from the expected noise distribution. This paper tries to address such practical issues connected with the implementation of the null-stream veto in the burst-data-analysis using a network consisting of two co-located interferometric detectors, like the two LIGO detectors [2] in Hanford, WA. The detectors are allowed to have calibration uncertainties and correlated noise components. In Section 2, we briefly review the veto method in the case of two co-located detectors. In Section 3, we estimate the effect of calibration uncertainties in the null-stream veto, and in Section 3, we lay out and demonstrate a formulation to overcome this effect.

## 2. The null-stream veto

In the case of detectors placed widely apart, the null-stream is a function of the antenna patterns, and hence, the source-position [1]. But in the case of two co-located detectors, the null stream is particularly simple. If  $h_1(t)$  and  $h_2(t)$  denote the properly calibrated time series data from the two detectors, the null-stream is just [10]:

$$n(t) = h_1(t) - h_2(t), \quad (1)$$

or, in discrete notation

$$n_j = h_{1_j} - h_{2_j}, \quad (2)$$

where  $h_{1_j}$  and  $h_{2_j}$  are the sampled versions of  $h_1(t)$  and  $h_2(t)$ . At the time of a set of coincident triggers, we construct the null-stream  $n_j$ . Let  $\tilde{N}_k$  denote the discrete Fourier transform (DFT) of  $n_j$  computed using  $L$  samples of the data. We assume that the real and imaginary parts of  $\tilde{N}_k$  are derived from a multivariate Gaussian distribution of mean zero  $\ddagger$  and variance  $\sigma_k^2$ . Following [6, 10], we compute the ‘excess power’ statistic from the null-stream:

$$\epsilon = \sum_{k=m}^{m+M} P_k, \quad P_k = \frac{|\tilde{N}_k|^2}{\sigma_k^2}. \quad (3)$$

It can be shown that  $\epsilon$  will follow a  $\chi^2$  distribution of  $2M$  degrees of freedom in the case of a non-windowed DFT. But in the case of a windowed DFT,  $P_k$  are not *independent*  $\chi^2$  variables, and hence  $\epsilon$  will *not* follow a  $\chi^2$  distribution [14]. But, we note that the  $\chi^2$  distribution is a special case of the Gamma distribution. It can be shown that, to a very good approximation,  $\epsilon$  will follow a Gamma distribution with scale parameter  $\alpha$  and shape parameter  $\beta$ . These parameters are related to the mean  $\mu_\epsilon$  and variance  $\sigma_\epsilon^2$  of the distribution of  $\epsilon$  by

$$\alpha = \left(\frac{\mu_\epsilon}{\sigma_\epsilon}\right)^2, \quad \beta = \frac{\sigma_\epsilon^2}{\mu_\epsilon}. \quad (4)$$

In order to estimate the parameters of the expected Gamma distribution, we generate a population of  $\epsilon$  from stationary data (i.e., data not containing the burst event under investigation, but surrounding it). To be explicit, we divide the data into a number of segments each length  $L$  and compute  $\epsilon$  from each of these segments. From that population,  $\mu_\epsilon$  and  $\sigma_\epsilon^2$  can be estimated, and hence  $\alpha$  and  $\beta$ .

It is known that the maximum signal-to-noise ratio (SNR) for the excess power statistic is achieved when the time-frequency volume used to compute the statistic is equal to the actual time-frequency volume of the signal [6]. Since the duration and bandwidth of the burst is estimated by the burst detection algorithm itself, this information is used to decide on the length ( $L$ ) of the data used to compute  $\tilde{N}_k$  and the bandwidth over which  $P_k$  is summed over.

If the  $\epsilon$  computed from the segment containing the burst is greater than a threshold, we veto the trigger. The threshold,  $\tau$ , giving a false-dismissal (‘false-veto’) probability of  $\gamma$  can be found by

$$\gamma = \int_\tau^\infty f(x; \alpha, \beta) dx, \quad (5)$$

where  $f(x; \alpha, \beta)$  is the probability density of the Gamma distribution with parameters  $\alpha$  and  $\beta$ .

### 2.1. Software injections

Let us define some terminology. The false-dismissal probability is the *probability* of an actual GW burst being falsely vetoed, and the ‘false-veto fraction’ is the fraction of GW bursts that are *actually* vetoed using this method. As a sanity check, we estimate the false-veto fraction by injecting some prototype gravitational-waveforms into two data streams of Gaussian white-noise and performing the analysis. If all of

$\ddagger$  If the real and imaginary parts of  $\tilde{N}_k$  are derived from a non-zero-mean Gaussian distribution, one can always convert them to mean-zero Gaussian variables by subtracting the sample mean  $\mu_k$  from them.

our assumptions are true, the fraction of vetoed events among the injections should be equal to the chosen false-dismissal probability.

The injected waveforms are Gaussian-modulated sinusoidal waveforms, of the form:

$$\hat{h}(t) = \hat{h}_{\text{RSS}} \left( \frac{2f_0^2}{\pi} \right)^{1/4} \sin[2\pi f_0(t - t_0)] \exp[-(t - t_0)^2/\tau^2], \quad (6)$$

where  $f_0$  is the central frequency of the waveform (randomly chosen from the set {153, 235, 361, 554, 849, 1053, 1245, 1534, 1856} Hz) and  $t_0$  is the time corresponding to the peak amplitude. We setup the envelope width as  $\tau = 2/f_0$ , which gives durations of approximately 1-20 ms. The corresponding quality factor is  $Q \equiv \sqrt{2}\pi f_0 \tau = 8.9$  and bandwidth is  $\Delta f = f_0/Q \simeq 0.1f_0$ . The quantity  $\hat{h}_{\text{RSS}}$  is the root-sum-squared (RSS) amplitude:

$$\left[ \int_{-\infty}^{\infty} \hat{h}^2(t) dt \right]^{1/2} = \hat{h}_{\text{RSS}}. \quad (7)$$

The  $\hat{h}_{\text{RSS}}$  is randomly chosen from the logarithmically-spaced interval  $(5 \times 10^{-22}, 1 \times 10^{-19})$ . The amplitude spectral density (ASD) of the noise in the two data streams is chosen to be  $1 \times 10^{-22}/\sqrt{\text{Hz}}$  and  $2 \times 10^{-22}/\sqrt{\text{Hz}}$ . We define the combined SNR,  $\rho$ , by

$$\rho^2 = \rho_1^2 + \rho_2^2, \quad (8)$$

where  $\rho_1$  and  $\rho_2$  are the optimal SNRs  $\S$  in detecting the bursts in the two data streams, and quote this quantity while discussing the results.

The veto analysis is performed with different thresholds. The fraction of vetoed events is plotted against the false-dismissal probability corresponding to the chosen threshold in Figure 1 (left). It can be seen that the estimated false-veto fraction is in very good agreement with the predicted false-dismissal probability.

### 3. Calibration uncertainties

So far, we have been assuming that the two data streams are perfectly calibrated. But, due to various limitations in the calibration procedure, the calibration of present-day interferometers can be subject to uncertainties of a few percent in amplitude and a few degrees in phase. This means that the null-stream constructed from the data containing actual GW triggers can contain some residual signal, and the computed statistic can vary from the expected distribution. This will result in a different false-dismissal probability than the one predicted by the hypothesis test.

It can be shown that we see approximately the same residual signal power in the null-stream for both a 10% relative amplitude error and a 10 degree relative phase error; therefore, in principle, we need to consider both of these effects. However, it is not easy to conceive of a simple model for the possible relative phase error between two co-located detectors (since such errors most probably arise due to inaccuracies in the calibration process and will therefore be frequency dependent)  $\parallel$ . It is, however, easy to think of a simple model for one possible source of relative amplitude calibration

$\S$  The optimal SNR  $\rho$  in detecting a signal  $h(t)$  buried in the noise is defined by  $\rho^2 = 4 \int_0^\infty |\tilde{H}(f)|^2 df / S_n(f)$  where  $\tilde{H}(f)$  is the Fourier transform of the signal and  $S_n(f)$  is the one-sided PSD of the detector noise.

$\parallel$  One another possible source of relative phase error would be a time-offset between the two data streams. Although it is unlikely that such an error exists at any significant level, it would be possible to include this in the following analysis if necessary.

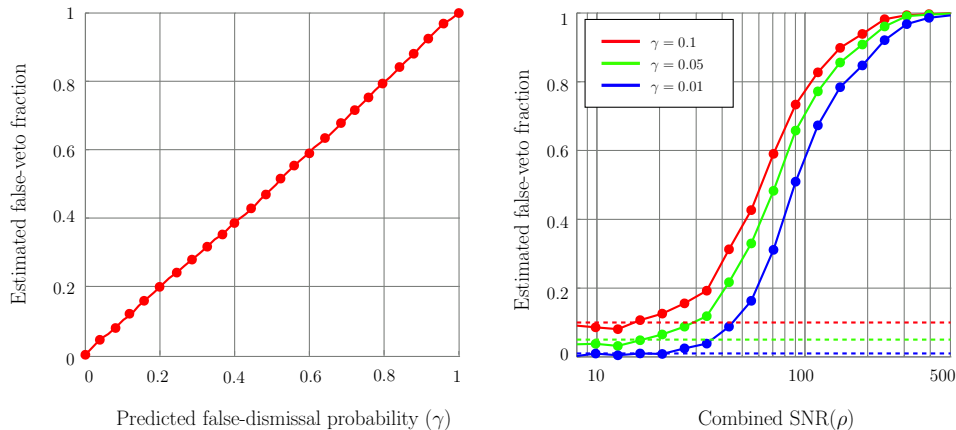


**Figure 1.** [Left]: Estimated false-veto fraction plotted against the predicted false-dismissal probability, assuming that the two detectors are perfectly calibrated. [Right]: Estimated false-veto fraction in the presence of  $\pm 10\%$  calibration uncertainty, plotted against the combined SNR of the injections, for three different values of the predicted false-dismissal probability ( $\gamma$ ). The three dashed lines show the predicted values of the false-dismissal probability in the absence of calibration uncertainties.

error. Suppose we know the absolute calibration of each detector to some accuracy. Then we have the possibility that the difference between the two data streams contains a systematic calibration error that would be independent of frequency. We explore a way to deal with this type of error in the rest of this paper.

As a simple model, we assume that the frequency-dependence of the calibration error is negligible, and that the calibration error is a constant scaling factor over short time-scales (of the order of seconds). In the context of this analysis, we can assume that one detector is perfectly calibrated and the other is calibrated with a wrong scaling factor, i.e.,

$$\begin{aligned} h_1(t) &= n_1(t) + \hat{h}(t), \\ h_2(t) &= n_2(t) + (1 + \delta) \hat{h}(t), \end{aligned} \quad (9)$$

where  $n_1(t)$  and  $n_2(t)$  are the detector noises in which a gravitational waveform  $\hat{h}(t)$  is present.  $\delta$  is the relative calibration error which is assumed to be a real quantity and is constant over short time-scales.

In order to estimate the effect of calibration error in the false-dismissal probability, injections are done simulating a relative calibration error of  $\delta = \pm 0.1$  between the two data streams. The fraction of the vetoed events among the injections is shown in the right plot of Figure 1 as a function of the combined SNR of the injections. Different curves in the plot represent three different values of the predicted false-dismissal probability ( $\gamma$ ). It can be seen that the estimated false-veto fraction raises to alarmingly high values for strong signals.

### 3.1. Dealing with calibration uncertainties

In this section we formulate a strategy to reduce the effect of calibration errors in the false-dismissal probability. We construct the following linear combination of the data

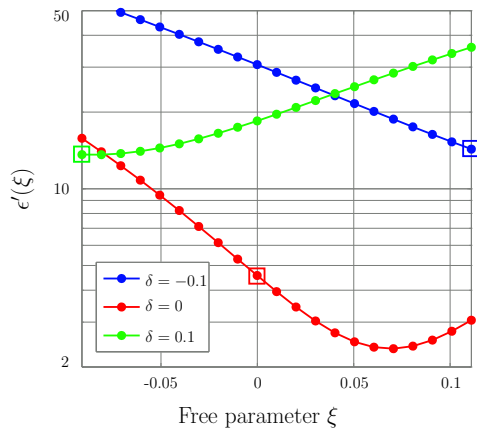


**Figure 2.** The excess-power statistic  $\epsilon'(\xi)$  constructed from null-stream  $n'(t; \xi)$  plotted against the free parameter  $\xi$ , for three different values of  $\delta$ . We assume that the maximum possible absolute value of  $\delta$  is 0.1.  $\epsilon'(-\delta/(1+\delta))$  for each curve is marked with a square. It can be seen that the minimum value of  $\epsilon'(\xi)$  is less than, or equal to  $\epsilon'(-\delta/(1+\delta))$ .

streams by introducing a free parameter,  $\xi$ , in the null-stream construction, i.e.,

$$n'(t; \xi) = h_1(t) - (1 + \xi) h_2(t). \quad (10)$$

Substituting for  $h_1(t)$  and  $h_2(t)$  from Eq.(9) gives,

$$n'(t; \xi) = n(t; \xi) - (\delta + \xi + \xi \delta) \hat{h}(t), \quad (11)$$

where

$$n(t; \xi) = n_1(t) - (1 + \xi) n_2(t), \quad (12)$$

is the ‘perfect’ null-stream. We can ‘tune’ the parameter  $\xi$  such that the residual signal disappears in Eq.(11). This is accomplished by minimizing the ‘excess power’ in  $n'(t; \xi)$  by varying  $\xi$  over an interval.

As described in Section 2, the null-stream  $n(t; \xi)$  is divided into a number of short segments and the DFT of each segment is computed. It may be noted that in all segments except the one containing the burst,  $n'(t; \xi) = n(t; \xi)$ , because the signal is absent in these segments. We denote the DFT of  $n(t; \xi)$  and  $n'(t; \xi)$  by  $\tilde{N}_k(\xi)$  and  $\tilde{N}'_k(\xi)$ , respectively. The mean,  $\mu_k(\xi)$ , and variance,  $\sigma_k^2(\xi)$ , of  $\tilde{N}_k(\xi)$  are estimated from the neighboring segments of the one containing the burst. These are the moments of the expected distribution of  $\tilde{N}'_k(\xi)$  in the absence of the burst.  $\tilde{N}_k(\xi)$  is converted to a mean-zero Gaussian variable by subtracting the sample mean  $\mu_k(\xi)$  from it. The test statistic  $\epsilon'(\xi)$  is computed from the segment of  $n'(t; \xi)$  containing the burst:

$$\epsilon'(\xi) = \sum_{k=m}^{m+M} P'_k(\xi), \quad P'_k = \frac{|\tilde{N}'_k(\xi)|^2}{\sigma_k^2(\xi)}. \quad (13)$$

We minimize  $\epsilon'(\xi)$  by varying  $\xi$  over an interval  $(\xi_{\min}, \xi_{\max})$  ¶. The boundary of the parameter-space can be fixed as

$$\xi_{\min} = \frac{-\delta_{\max}}{1 + \delta_{\max}}, \quad \xi_{\max} = \frac{\delta_{\max}}{1 - \delta_{\max}}, \quad (14)$$

¶ It is important to note that we minimise the *excess-power*,  $\epsilon'(\xi)$ , in the null-stream, and not the *total power*,  $n'^2(t; \xi)$ . In the later case, if there are correlated noise in  $h_1(t)$  and  $h_2(t)$ ,  $\xi$  can take values which will minimise the correlated noise components in  $n'(t; \xi)$  instead of the residual signal.

were  $\pm\delta_{\max}$  is the maximum allowed value of the calibration uncertainty. When  $\xi \rightarrow -\delta/(1+\delta)$ , the residual signal in the null-stream cancels out, and  $\epsilon'(\xi) \rightarrow \epsilon(\xi)$ , where

$$\epsilon(\xi) = \sum_{k=m}^{m+M} P_k(\xi), \quad P_k = \frac{|\tilde{N}_k(\xi)|^2}{\sigma_k^2(\xi)}, \quad (15)$$

which falls in to an expected Gamma distribution in the case of GW bursts.

Since  $\epsilon$  is quadratic in  $\tilde{N}'_k$ , apart from  $|\tilde{N}_k|^2$  and  $|(\delta + \xi + \xi\delta)\hat{H}_k|^2$ , it contains also the cross-terms. This means that the minimum value of  $\epsilon'(\xi)$  could be less than  $\epsilon(\xi)$ . This is illustrated in Figure 2, for three different values of  $\delta$ . Thus, the obtained false-dismissal probability could be less than what is predicted by the hypothesis test. Since the cross-terms depend upon the actual value of  $\delta$ , this adds an error-bar to the false-dismissal probability. *But it may be noted that the actual false-dismissal probability is always less than (or equal to) what is predicted by the hypothesis test.*

### 3.2. Software injections with simulated calibration errors

We generate two data streams with a simulated relative calibration error  $\delta$  according to Eq.(9) and perform the veto analysis, assuming that the  $|\delta_{\max}| = 0.1$ . The minimisation of  $\epsilon(\xi)$  is carried out using an optimised minimisation algorithm. The analysis is performed for three different values (-0.1, 0, 0.1) of  $\delta$  and the false-veto fractions corresponding to different thresholds are estimated in each case (in all cases, we assumed that  $|\delta_{\max}| = 0.1$ ). The mean value (of the three simulations) of the false-veto fraction corresponding to each threshold is plotted against the corresponding false-dismissal probability in Figure 3 (left). The extremum values corresponding to each threshold are used to generate the error-bars. It can be seen that the estimated false-veto fraction is always less than or equal to the predicted false-dismissal probability.

The real figure-of-merit of a veto method is its ability to reject spurious events with a given false-dismissal probability. But, given that the probability density of the noise transients are not known *a priori*, there is no rigorous way of estimating the ‘rejection power’ of the veto. The best we can do is to estimate the ability of the veto to reject a given glitch population. As a plausible estimation, we inject a population of sine-Gaussian waveforms with random parameters into two data streams. We then perform the veto analysis after choosing different thresholds. The estimated rejection power is plotted against the false-dismissal probability in Figure 3 (right). Since the ‘excess power’ in the null-stream is proportional to the individual SNRs of the bursts in the two data streams, the rejection power is also proportional to the SNR. Each curve in the figure corresponds to a particular range of SNR  $\rho$  (see Eq.(8)). This suggests that veto efficiencies of  $\geq 90\%$  can be achieved with a false-dismissal probability of  $\simeq 1\%$  for spurious noise transients with  $\rho \geq 10$ .

## 4. Summary

The null-stream constructed from the data of multiple GW detectors can be used to distinguish between actual GW triggers and spurious noise transients in the search for GW bursts using a network of detectors. The biggest source of error in the analysis comes from the fact that the present-day detectors are subject to calibration uncertainties. In this paper we have proposed an implementation of

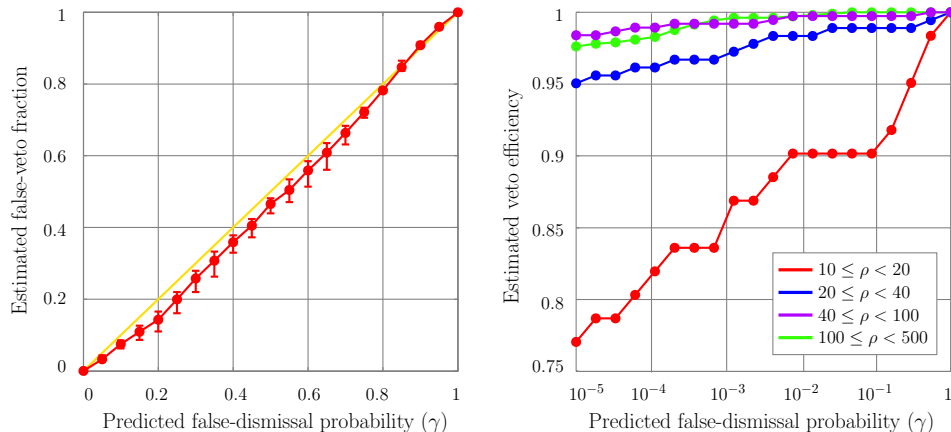


**Figure 3.** [Left]: Estimated false-veto fraction plotted against the predicted false-dismissal probability. The relative calibration between  $h_1(t)$  and  $h_2(t)$  is assumed to be between  $-0.1 \leq \delta \leq 0.1$ . [Right]: Rejection power of the veto plotted against the predicted false-dismissal probability. Each curve in the plot corresponds to a particular range of SNR.

the null-stream veto in the search for GW bursts in the data of two co-located interferometers. We have estimated the effect of calibration uncertainties in the veto analysis by performing software injections in Gaussian noise with simulated calibration errors. A strategy is proposed to minimize this effect, assuming a simple model for the amplitude calibration-error and neglecting the errors in the phase calibration. This is done by introducing an additional free parameter in the null-stream combination and minimizing the excess-power in the null-stream. Finally, we compared the estimated fraction of falsely-vetoed GW-like injections with the predicted false-dismissal probability and found that the estimated fraction has a good agreement with the prediction. We also estimate the rejection power of the veto as a function of the false-dismissal probability.

## Acknowledgments

The authors are grateful to Bruce Allen, Peter Shawhan, Bernard Schutz, Linqing Wen and members of the LIGO Scientific Collaboration's Working Group on Burst Sources for useful discussions.

- [1] *Near optimal solution to the inverse problem for gravitational-wave bursts*, Y Gürsel and M Tinto, *Phy. Rev. D.* **40**, 3884 (1989).
- [2] *Status of the LIGO detectors*, D Sigg (for the LIGO Scientific Collaboration), *Class. Quantum Grav.* **23** (2006) S51-S56.
- [3] *The status of Virgo*, F Acernese *et al* , *Class. Quantum Grav.* **23** (2006) S63-S69.
- [4] *Status of the GEO 600 detector*, H Lück *et al* , *Class. Quantum Grav.* **23** (2006) S71-S78.
- [5] *Current status of the TAMA300 gravitational-wave detector*, Masaki Ando and the TAMA Collaboration, *Class. Quantum Grav.* **22** No 18 (21 September 2005) S881.
- [6] *Excess power statistic for detection of burst sources of gravitational radiation*, W G Anderson, P R Brady, J D E Creighton and É É Flanagan, *Phys. Rev. D* **63**, 042003 (2001).
- [7] *Time-frequency detection algorithm for gravitational wave bursts*, J Sylvestre, *Phys. Rev. D* **66**, 102004 (2002).
- [8] *A wavelet method for detection of gravitational wave bursts*, S Klimenko and G Mitselmakher, *Class. Quantum Grav.* **21** No 20 (21 October 2004) S1819-S1830.



- [9] *Coherent waveform consistency test for LIGO burst candidates*, L Cadonati, *Class. Quantum Grav.* **21** No 20 (21 October 2004) S1695-S1703.
- [10] *Coherent network detection of gravitational waves: the redundancy veto*, L Wen and B F Schutz, *Class. Quantum Grav.* **22** No 18 (21 September 2005) S1321-S1335.
- [11] *Null-stream veto for the network analysis of gravitational-wave bursts*, P Ajith, M Hewitson, I S Heng, L Wen and B F Schutz, in preparation (2006).
- [12] *Coherent network analysis technique for discriminating gravitational-wave bursts from instrumental noise*, S Chatterji, A Lazzarini, L Stein, P Sutton, A Searle and M Tinto, LIGO Laboratory document number LIGO-P060009-00-E (2006); gr-qc/0605002.
- [13] *Using the null-stream of GEO 600 to veto transient events in the detector output*, M Hewitson and P Ajith, *Class. Quantum Grav.* **22** No 22 (21 November 2005) 4903-4912.
- [14] *The probability density of spectral estimates based on modified periodogram averages*, P E Johnson and D G Long, *IEEE Trans. on Signal Processing* **47**, 1255 (1999).